Journal of Engg. Research Vol.10 No. (2A) pp. 136-160 DOI: 10.36909/jer.13285

The impact of PV generation and load types on the impedance relays during both balanced and unbalanced faults

Rashad M. Kamel* and Heba M. Abdullah*,**

** Electrical Engineering Department College of Engineering and Petroleum, Kuwait University, Kuwait.*
*** Electrical Engineering Department College of Engineering, Qatar University, Doha.*
** Corresponding Author: rmkamelm@gmail.com*

Submitted *:* 23/02/2021
Revised *:* 20/06/2021
Accepted *:* 04/07/2021

ABSTRACT

Photovoltaic (PV) power generation and the types of connected loads both have an effect on protective impedance relays' readings. This paper investigates this effect in a real distribution system installed in the State of Kuwait. It is found that both the dynamic loads and the PV plants have considerable effects in the relay impedance value, which vary according to the load type, PV connection, and fault location. Both single phases to ground fault (unsymmetrical fault) and three-phase fault (symmetrical fault) are investigated. When single line to ground fault occurs at the PV bus (far from relay location), the dynamic loads increase the relay impedance, while the PV plant decreases the relay impedance. When a single phase to ground fault occurs at the relay bus (load bus), the dynamic load decreases the relay impedance, and the PV plant increases it. For a three-phase to ground fault at the relay bus, both dynamic load percentages and PV plant power generation have no effect on the protective relay impedance readings. At this condition, the relay impedance totally depends on the fault resistance. The main finding of this paper is that both the load type (especially dynamic load) and the PV plant have dominant effects on the protective impedance relay reading and setting. The distribution system planners and operators must consider the PV plant and types of load during designing, setting, and adjusting the protective impedance relays. The most important point in this paper is considering real case study. This means that the obtained results are more realistic than the assumed system in the other research.

Keywords: PV; Static loads; Dynamic loads; Impedance relay; Relay setting; Fault resistance; Symmetrical and unsymmetrical faults.

1. INTRODUCTION

For the past years, solar energy generation has increased significantly. The aim of PV integration is to reduce the carbon emissions by reducing the generated power from conventional fossil fuel power plants. Many studies are focusing on the impacts of PV distributed generation (PVDG) on the distribution side, which have various issues on the power system because of its interment nature. Some of the complications caused by PVDG are harmonics, voltage and frequency variations and power imbalance. The issues related to PV penetration and its impacts on the power system are reviewed in (Karimi et al., 2016) and (Eltawil and Zhao, 2010).

Photovoltaic designs, operations and maintenances are reviewed in (Hernández-Callejo et al., 2019). Monitoring Photovoltaic distributed generation (PVDG) is necessary because of the intermittent nature of PV where it requires real-time performance monitoring for system control and protection (Madeti and Singh, 2017a). PV power flow can be reversed where it can cause voltage rise unlike conventional power plants (Masters, 2002).

A more recent study distinguishes between voltage increasing and voltage decreasing of a power system with PV reverse flow which depends on the impedance of the line and the PV system power factor (Iioka et al., 2019). It is proposed by (Mortazavi et al., 2015) to utilize impedance measurements of the distance relays for monitoring power system loading and PV system power penetration. The measured apparent impedance is the combination of both the load and line impedances.

Integrating DG to the conventional power grid can impact protection system coordination and, therefore, requires modified protection schemes (Darwish et al., 2013). The impact of high PV penetration is modelled and studied for a balanced three phase system in (Bracale et al., 2017). Interconnecting PVDG to the power system can cause changes in the apparent impedances and affect the function of distance relays (Sorrentino et al., 2018). The protection challenges are review in (Telukunta et al., 2017). A new approach to adjust protection relays considers fault current limiters with minimum number of relays to be adjusted (Ibrahim et al., 2017). A design procedure for over current relay with renewable generation is proposed in (Chen, 2017). False detection caused by distribution of non-linear loads is studied in (Soheili et al., 2018). The effect of Static Synchronous Series Compensator (SSSC) on distance relay calculation is investigated in (Ghorbani et al., 2012). Different types of fault detections for both ac and dc sides of the PV power systems are reviewed in (Madeti and Singh, 2017b).

A study in (Kim and Aggarwal, 2006) suggests utilizing the distance relay for monitoring the transmission line operating condition. An online-measurement procedure for improving the distance relay accuracy is proposed which can be used during normal or fault conditions. The protection relay setting depends on the accurate phasor measurements of the voltage and current.

To the best of the authors' knowledge, limited published work deals with the impact of load types on the impedance relay reading combined with DG. Also, the effects of DGs especially the PV on the protective relay readings and settings are not investigated in detail, where the published work mostly assumed distribution system loads as constant power static loads and did not consider other load types such as rotating loads (dynamic loads) combined with PVDG.

In latest work related to this topic, a study by (Mishra et al., 2021) considers a 39-bus system with a 300 MW renewable plant modelled in PSCAD. The study investigates a large PV plant and at one location in the power system. The authors proposed an adoptive relay technique that measures the line impedance up to the fault point and obtains a deviation angle to adjust the relay setting.

The main goal of this study is a detailed investigation and analysis of the effects of load types with PVDG on the impedance relay reading and setting. This paper considers both rotating and static load types. In addition, the faults are simulated at different location (at PV bus or at load bus) and their effects on the relay reading and setting are studied in detail. The remaining of the paper is organized as follows:

Section 2 describes the real distribution system with installed PV (10 MWp) and real loads. Section 3 deals with a mathematical analysis and description of different types of load. Also, the influence of the PV on the fault current of the distribution system has been described in section 3. Section 4 analyzes the performance of the impedance protective relay under symmetrical and unsymmetrical faults. Section 5 displays the obtained results with different

load types and with or without PV under both symmetrical and unsymmetrical faults and reports the main finding of paper. Conclusions are reported in section 6.

2. METHODOLOGY

2.1 Flow Chart

In this section, we summarize the methods used for investigating the effect of both PV and load type on the impedance relay. We generalize the procedure into the chart in Fig. 1 so it can be a useful tool for other researcher and for future studies. The first step is to model the power systems involved in the study including the distribution system and the solar power system. Then, we model the overall power system in ETAP software in order to perform the short circuit analysis in step 4. different scenarios are under investigation to study the effect of fault location, fault impedance, fault type, and load type on the obtained results.

Figure 1. Summary of calculation methodology.

2.2 Architecture of the Investigated Distribution Network with PV and Loads

A 10MWp grid connected PV plant to one of the Kuwait Oil Company's (KOC) electrical distribution system which supplies electricity to oil pump at the Umm-Gudair field, West Kuwait (Abdullah et al., 2016) . The distribution system which contains the PV plant is shown in Fig. 2b. The main grid feeding the load bus (KOC bus) is the "Minagish B" substation. Four feeders (incomers) coming from the "Minagish B" substation (11 kV) and represent bus 1 (Fig. 2b). Three of the four incomers are continuous, and one is spare for redundancy. The four incomers are operating with closed breakers. The 11 kV load bus is Bus 2 (Fig. 2). The PV plant is installed at Bus 3. The distances between different buses are shown in Fig. 2 (Abdullah et al., 2016).

3. MATHEMATICAL ANALYSIS AND MODELLING OF DIFFERENT LOADS AND PV INTERFACING INVERTER

3.1 Different Load Types

There are two main types of the electrical loads, static and dynamic (rotating) loads. The description and mathematical modelling of the two load types are described in the following subsections.

3.2 Static Load Modelling

A static load model is the characteristics of the load as a function of the voltage and frequency (IEEE Task Force on Load Representation for Dynamic Performance, 1993), (Abdullah et al., 2016), and (Kamel and Nagasaka, 2015). The static load real power (P) and imaginary power (Q) components are considered separately. The dependency of real power (P) and imaginary power (Q) on the magnitude of the voltage (V) can be calculated as follows (Kamel and Nagasaka, 2015) :-

$$P = P_o (\bar{V})^a \,, \tag{1}$$

$$Q = Q_o (\bar{V})^b \,, \tag{2}$$

$$\bar{V} = \frac{V}{V_o}, \tag{3}$$

where P_o, Q_o, V_o represent initial conditions of the real, imaginary powers and voltage, respectively. The a and b are the parameters of the load model. Three models are available as follows (Kundur, 1994), and (Kamel and Nagasaka, 2015):

a) Static load with constant power when the parameters $a = b =$ zero.
b) Static load with constant impedance when the parameters $a = b = 1$.
c) Static load with a constant current when $a = b = 2$.

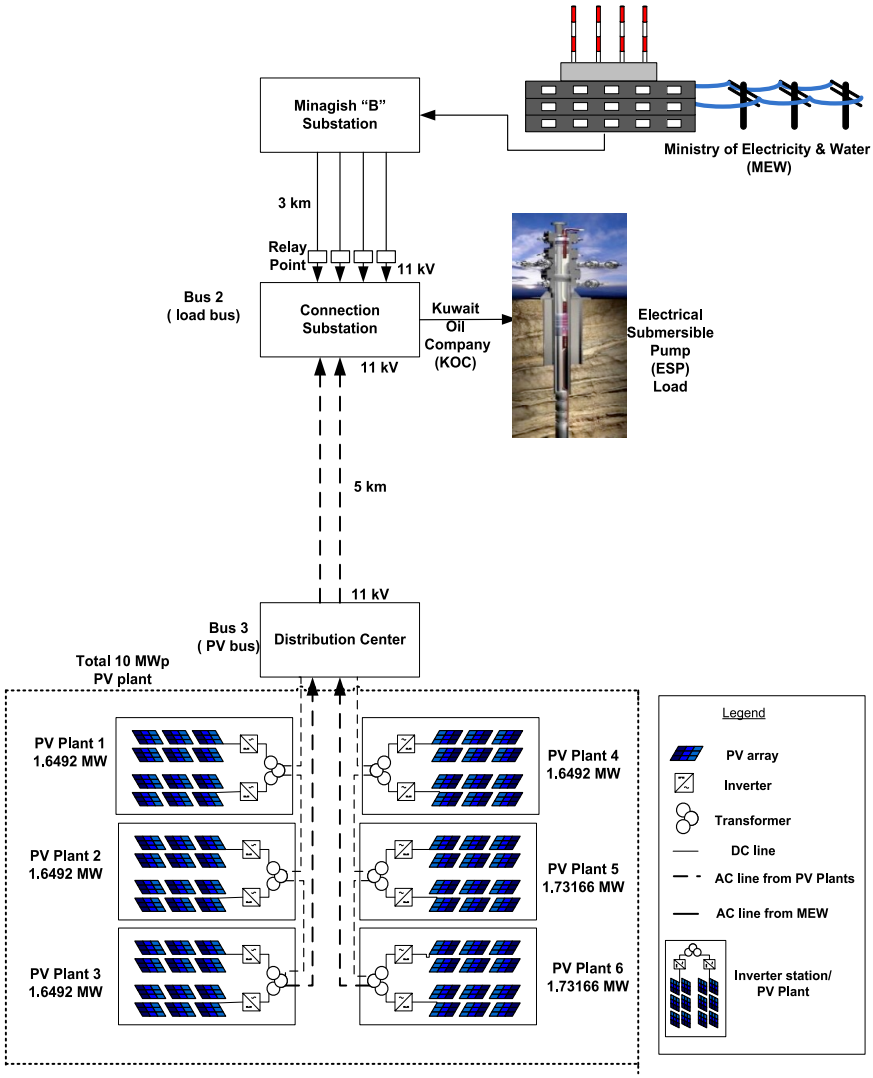

Figure 2. Case study, power system configuration and single line diagram (Abdullah et al., 2016).

The voltage dependency of load model is given by the following equation:

$$P = P_o [\, p_1 \bar{V}^{\,2} + p_2 \bar{V} + p_3], \tag{4}$$

$$Q = Q_o [\, q_1 \bar{V}^{\,2} + q_2 \bar{V} + q_3] \tag{5}$$

The effect of frequency on the load characteristics is given by the following equation:

$$P = P_o (\bar{V})^a (1 + k_{pf} \Delta f), \tag{6}$$

$$Q = Q_o (\bar{V})^b (1 + k_{qf} \Delta f), \tag{7}$$

Or

$$P = P_o [\, p_1 \bar{V}^{\,2} + p_2 \bar{V} + p_3](1 + k_{pf} \Delta f), \tag{8}$$

$$Q = Q_o [\, q_1 \bar{V}^{\,2} + q_2 \bar{V} + q_3](1 + k_{qf} \Delta f), \tag{9}$$

where Δf represents the frequency deviation ($f - f_o$). Typically, k_{pf} is between 0 to 3.0 and k_{qf} is between 0 to -2.0 (Concordia and Ihara, 1982).

A general model for static load is given as follows (Kamel and Nagasaka, 2015), and (Kundur et al., 1993):

$$P = P_o [P_{ZIP} + P_{EX1} + P_{Ex2}], \tag{10}$$

Where

$$P_{ZIP} = p_1 \bar{V}^{\,2} + p_2 \bar{V} + p_3, \tag{11}$$

$$P_{EX1} = p_4 (\bar{V})^{a1} (1 + k_{pf1} \Delta f), \tag{12}$$

$$P_{EX2} = p_5 (\bar{V})^{a2} (1 + k_{pf2} \Delta f), \tag{13}$$

$$Q = Q_o [Q_{ZIP} + Q_{EX1} + Q_{Ex2}], \tag{14}$$

$$Q_{ZIP} = q_1 \bar{V}^{\,2} + q_2 \bar{V} + q_3, \tag{15}$$

$$Q_{EX1} = q_4 (\bar{V})^{b1} (1 + k_{qf1} \Delta f), \tag{16}$$

$$Q_{EX2} = q_5 (\bar{V})^{b2} (1 + k_{qf2} \Delta f) \tag{17}$$

3.1.2 Modelling of Dynamic Loads

Induction (asynchronous) motors represent the widely used dynamic loads. Typically, asynchronous motors dissipated 50% to 70 % of the total power system energy **(Kundur et al., 1993)**. Fig. 3 shows the asynchronous machine equivalent circuit referred to the machine stator side.

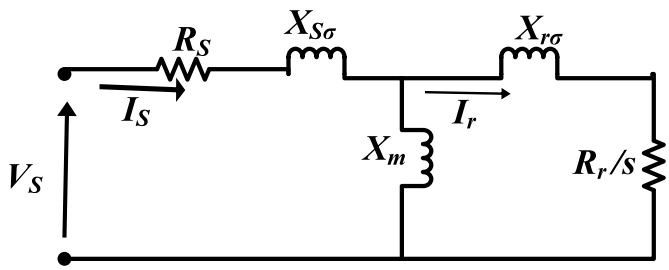

Figure 3. Equivalent circuit refereed to stator of the asynchronous machine.

In Fig. 3, S is the slip speed of the machine. The typical value of asynchronous machine running slip ranges between 0 to 3.0% (Kamel and Nagasaka, 2015), and (Kamel, 2014) .

The initial value of the injected fault current by the induction machine (rotating load) is approximately equal to the machine locked rotor current. For the balanced fault (three phase fault), the mathematical equation which estimates the contribution of the asynchronous machine is given as follows (Kamel and Nagasaka, 2015) , and (Morren and de Haan, 2007):

$$i(t) = \frac{\sqrt{2} V_S}{X_S^-} [e^{-\frac{t}{\tau_S^-}} \sin(\alpha) - (1-\sigma) e^{-\frac{t}{\tau_r^-}} e^{j\omega t} \sin(\omega t + \alpha)], \tag{18}$$

where

α is the voltage phase angle at the instant of fault occurrence.

σ is the flux leakage factor,

$X_S^- = \omega L_S^-$ is the transient reactance of asynchronous machine stator.

τ_S^- and τ_r^- are the machine stator and rotor time constants, and

ω is frequency in radians per second.

The transient reactance $\bar{X}_S$ and $\bar{X}_r$ of the machine stator and rotor can be evaluated as (Kamel and Nagasaka, 2015), (Morren and de Haan, 2007), and (Sulawa et al., 2007):

$$\bar{X}_S = X_{S\sigma} + \frac{X_{r\sigma} X_m}{X_{r\sigma} + X_m}, \tag{19}$$

$$\bar{X}_r = X_{r\sigma} + \frac{X_{S\sigma} X_m}{X_{S\sigma} + X_m} \tag{20}$$

The transient time constants for stator and rotor and leakage factors are given by (Kamel, 2014) :

$$\tau_S^- = \frac{L_S^-}{R_S}, \tag{21}$$

$$\tau_r^- = \frac{L_r^-}{R_r}, \tag{22}$$

$$\sigma = 1 - \frac{L_m^2}{L_S L_r}, \tag{23}$$

$$L_S = L_{S\sigma} + L_m \text{ and } L_r = L_{r\sigma} + L_m \tag{24}$$

According to (Kamel and Nagasaka, 2015), the asynchronous machine peak fault current is estimated as

$$i_{S,\max} = \frac{\sqrt{2} V_S}{X_S^-} [e^{-\frac{T}{2\tau_S^-}} + (1-\sigma) e^{-\frac{T}{2\tau_r^-}}], \tag{25}$$

where T is the period time and is equal to reciprocal of f and f is the frequency of the grid (50 Hz).

From equation (25), the parameters of the machine are the dominant factors effecting the injected fault current by the dynamic load.

3.2 PV Interfacing Inverter Model

Fig. 2 shows the configuration of the investigated distribution network. As shown, the PV bus (bus 3) is connected to the network through inverters. During a fault event, the interfacing inverter behaves totally different than the synchronous machine in the classical power grid. The synchronous machine feeds extremely high fault current, near 500% to 700% of its rated (full load) current (Kamel, 2014). On the other hand, the interfacing inverter contains a current limiter to protect the inverter switches from the high fault current (Morren and de Haan, 2007) . The fault current of an inverter interfaced PV ranges from 110% to 200% of the rated current (Boutsika and Papathanassiou, 2008). In this paper, the PV inverters are represented by variable virtual impedances, which limit the fault currents to 200 % of the inverters' rated current (Abdel-Salam et al., 2012) .

4. PROTECTIVE IMPEDANCE RELAY PERFORMANCE DURING BOTH BALANCED AND UNBALANCED FAULTS

The most important protective relay in the power system is the distance relay. The distance relay measures the impedance by dividing the measured voltage over the measured current at the relay place and is subsequently called impedance relay.

4.1 Principles of the Protective Impedance Relay

Fig. 5 shows the principle of operation of the protective impedance relay. The relay divides the relay measured voltage ($V_{\mathrm{Re}lay}$) by the relay measured current ($I_{\mathrm{Re}lay}$) (Fig. 4). During normal operation (Fig. 5a), the relay impedance is very high ($Z_{\mathrm{Re}lay} = Z_L + Z_{Load}$). During a fault event (Fig. 5b), the load impedance is short circuited and the relay measures very low impedance.

4.2 Protective Impedance Relay Reading During All Fault Types

In the following subsections, the readings of the protective impedance relay during symmetrical (three phase) fault and unsymmetrical (single line to ground, double lines to ground and line to line) faults will be analyzed.

4.2.1 Impedance Relay Reading Under Phase Faults Neglecting Fault Resistance ($R_F = 0$)

The phase faults include the three phase and the phase to phase faults. During those fault types, the earth is not a part of the circuit. The reading of the impedance relay is calculated by dividing the two faulty phase voltages over the two faulty phase current **(Tleis, 2019)**, **(Anderson, 1995)**, **(Xu et al., 2010)**, and **(Tseng et al., 2003)**. During phase to phase fault, and three line to ground fault, the voltage and current can be estimated as in table 1 **(Tleis, 2019)**.

Table 1. voltages and currents during line to line and three line to ground faults (Tleis, 2019).

Fault Quantity	Three lines to ground fault (A-B-C)	Line to Line fault (B-C)
I_A	I^+	0
I_B	$a^2 I^+,\ a^2 = 1\angle 240$	$(a^2 - a)I^+,\ a = 1\angle 120$
I_C	$a\, I^+$	$(a - a^2)I^+$
V_A	$Z_L^+ I^+$	$2(Z_S^+ + Z_L^+)I^+$
V_B	$a^2 Z_L^+ I^+$	$(2a^2 Z_L^+ - Z_S^+)I^+$
V_C	$aZ_L^+ I^+$	$(2aZ_L^+ - Z_S^+)I^+$

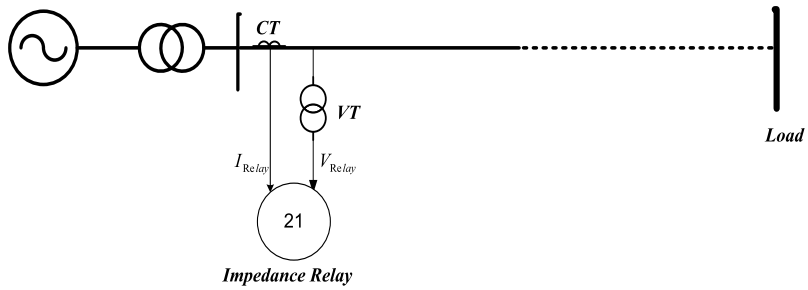

Figure 4. Principles and location of the impedance relay.

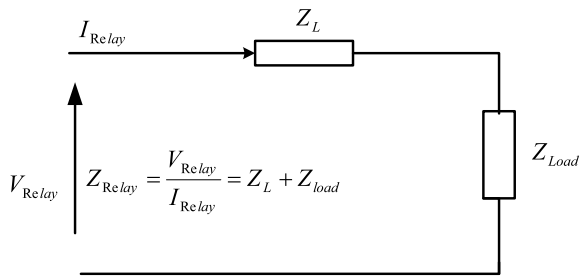

Figure 5a. Protective impedance relay during normal conditions.

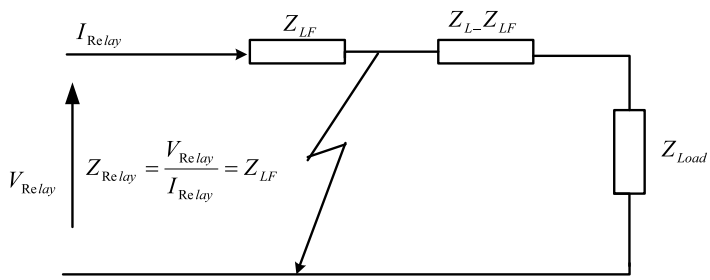

Figure 5b. Protective impedance relay during fault.

4.2.1.1 Protective Impedance Relay Reading During Line to Line Faults (Phase B to Phase C)

The relay reading is calculated as follows (Tleis, 2019):

$$Z_{Relay} = \frac{V_{BC}}{I_{BC}} \tag{26}$$

From table 1, Z_{Relay} is equal to

$$Z_{\text{Re}lay} = \frac{V_{BC}}{I_{BC}} = \frac{V_B - V_C}{I_B - I_C} = \frac{2(a^2 - a) Z_{LF}^{+} I^{+}}{(a^2 - a) I^{+}} = Z_{LF}^{+} \tag{27}$$

4.2.1.2 Protective Impedance Relay Reading During Three Line To Ground Faults (A-B-C)

The relay reading is calculated as

$$Z_{\text{Re}lay} = \frac{V_{AB}}{I_{AB}} \tag{28}$$

From table 1, $Z_{\text{Re}lay}$ is equal to

$$Z_{\text{Re}lay} = \frac{V_{AB}}{I_{AB}} = \frac{V_A - V_B}{I_A - I_B} = \frac{Z_{LF}^{+} I^{+} - a^2 Z_{LF}^{+} I^{+}}{I^{+} - a^2 I^{+}} = Z_{LF}^{+} \tag{29}$$

From equation (27-29), the protective impedance relay reading is equal to the positive sequence line impedance from the relay position until the short circuit location.

4.2.2 Protective Impedance Relay Reading Under Phase Faults Considering The Resistance of the Fault ($R_F \neq 0$)

Fig. 6a and Fig. 6b show three lines and line to line short circuit considering the resistance of the fault. The relay reading in existence of fault resistance can be calculated as (Nikolaidis et al., 2018):

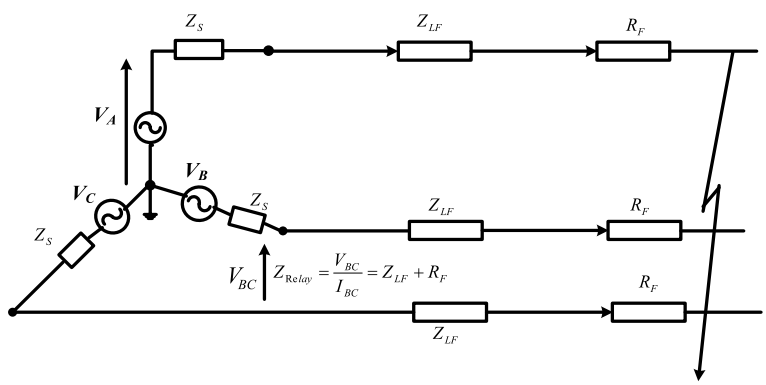

Figure 6a. Three phase fault with R_F.

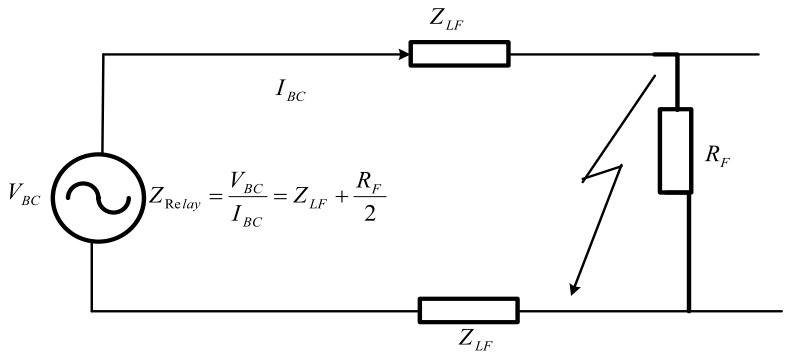

Figure 6b. line to line short circuit considering R_F.

4.2.2.1 Line to Line Fault (B-C) Considering the Resistance of the Fault ($R_F \neq 0$)

The relay impedance during phase to phase fault in existence of fault resistance can be estimated by (Tleis, 2019)

$$Z_{Relay} = \frac{V_{BC}}{I_{BC}} = Z_{LF}^{+} + \frac{R_F}{2} \tag{30}$$

4.2.2.2 Three Line to Ground Fault (A-B-C) ($R_F \neq 0$)

The relay impedance during three phase (balanced) fault in existence of the R_F in series with each phase (Fig. 6a) can be estimated by (Tleis, 2019)

$$Z_{Relay} = \frac{V_{AB}}{I_{AB}} = Z_{LF}^{+} + R_F \tag{31}$$

4.2.3 Protective Impedance Relay Reading During Earth Fault

The earth fault includes single line to ground and double lines to ground faults. During those two faults, the earth is apart from the circuit. Single phase to ground faults are the most common faults in the power system especially the distribution system. In the other side, double phase to ground faults rarely occur. Based on this fact, this paper investigates and highlights single phase to ground faults.

4.2.3.1 Single Line to Ground Fault Neglecting Fault Resistance ($R_F = 0$)

Fig. 7 represent schematic diagram of the single line to ground fault neglecting the fault resistance ($R_F = 0$). The relay impedance can be calculated as follows (Tleis, 2019):

$$Z_{Relay} = \frac{V_A}{I_A} = Z_{LF}^{+} \tag{32}$$

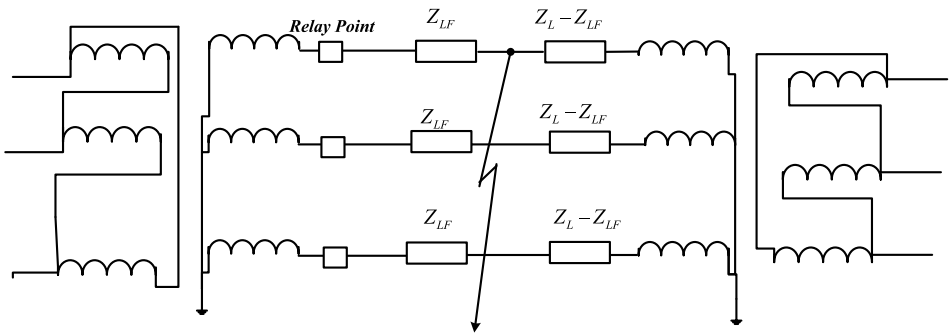

Figure 7. Solid ground single line to ground fault ($R_F = 0$).

4.2.3.2 Single Line to Ground Fault Considering R_F ($R_F \neq 0$)

Fig. 8a shows single line to ground fault in existence of R_F . Fig. 8b indicates its equivalent circuit. The impedance relay reading can be calculated by (Tleis, 2019)

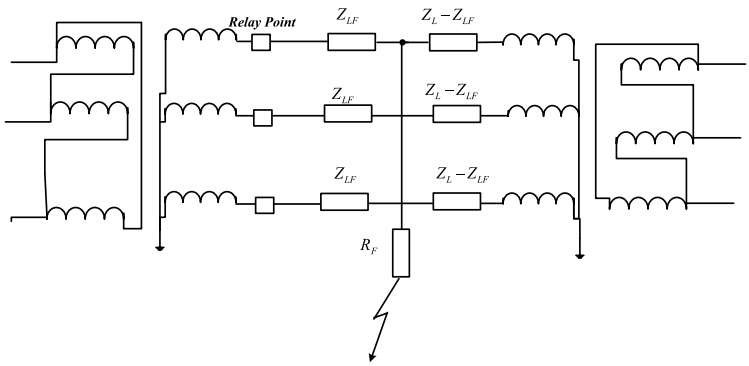

Figure 8a. Single line to ground fault with fault resistance.

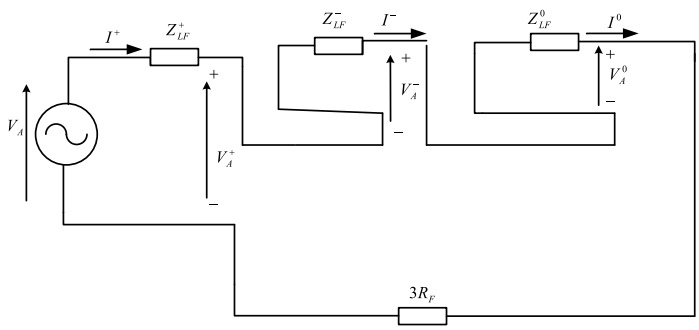

Figure 8b. Equivalent circuit of single line to ground fault considering fault resistance.

The faulty phase (phase A) voltage is given by (Tleis, 2019)

$$V_A = Z_{LF}^{+} I^{+} + Z_{LF}^{-} I^{-} + Z_{LF}^{0} I^{0} \tag{33}$$

The short circuit current is given by

$$I_A = I^{+} + I^{-} + I^{0}, \tag{34}$$

$$I^{+} = I^{-} = I^{0}, \tag{35}$$

$$I_N = I_A + I_B + I_C = I_A = 3I^{0} \tag{36}$$

It is known that $Z_{LF}^{+} = Z_{LF}^{-}$. Defining constant K equal to

$$K = \frac{Z_{LF}^{0}}{Z_{LF}^{+}} \tag{37}$$

From equations (33), (34), (36), and (37), the faulty phase voltage can be estimated as

$$V_A = Z_{LF}^{+}(I_A + (I_A + I_B + I_C) * \frac{(K-1)}{3} \tag{38}$$

The impedance relay reading can be calculated by dividing V_A over I_A as follows (Tleis, 2019):

$$Z_{\mathrm{Re}lay} = \frac{V_A}{I_A} = (1 + \frac{K-1}{3}) Z_{LF}^{+} \tag{39}$$

5. RESULTS AND DISCUSSIONS

To indicate the effect of both load type and PVDG on the protective impedance relay reading and setting, the investigated distribution network in (Fig. 2) is exposed to a single line to ground fault (the most common type in the distribution system) and three-lines to ground fault (the most severe fault), at the PV bus (bus 3) then at the load bus (bus 2). Four different main cases and 120 subcases are studied as follows:

1) Main case (1) includes 30 subcases, single line to ground fault at PV bus (bus 3) with and without PV, different percentages of dynamic load, and different values of R_F. The main case (1) and its subcases are indicated in table (2)

2) Main case (2) likes main case (1) except that three-line to ground fault instead of single line to ground fault occur at PV bus (bus 3).
3) Main case (3) is like main case (1) except that the fault location is at load bus (bus 2) instead of PV bus (bus 3).
4) Main case (4) is like main case (2) except that the fault location is at load bus (bus 2) instead of PV bus (bus 3).

The following results indicate the effects of load types (for all cases) and PVDG on the protective impedance relay reading and setting at all main studied cases and subcases.

Table 2. Studied main case (1) and its subcases.

Fault resistance	Single line to ground fault at PV bus (bus 3)					
R_F =0 ohm	Without PV			With PV		
	25 % dynamic load	50 % dynamic load	90 % dynamic load	25 % dynamic load	50 % dynamic load	90 % dynamic load
R_F =0.17 ohm	Without PV			With PV		
	25 % dynamic load	50 % dynamic load	90 % dynamic load	25 % dynamic load	50 % dynamic load	90 % dynamic load
R_F =0.3 ohm	Without PV			With PV		
	25 % dynamic load	50 % dynamic load	90 % dynamic load	25 % dynamic load	50 % dynamic load	90 % dynamic load
R_F =0.9ohm	Without PV			With PV		
	25 % dynamic load	50 % dynamic load	90 % dynamic load	25 % dynamic load	50 % dynamic load	90 % dynamic load
R_F =1.3ohm	Without PV			With PV		
	25 % dynamic load	50 % dynamic load	90 % dynamic load	25 % dynamic load	50 % dynamic load	90 % dynamic load

5.1 Single Line to Ground Fault at PV Bus Under Different Dynamic Load Percentages with and Without PV (different R_F)

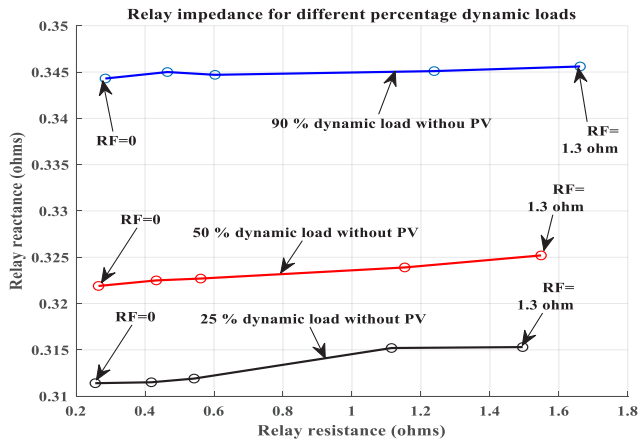

Figure 9. Relay impedance at different dynamic load percentages without PV.

Fig. 9 shows the protective impedance relay resistance and reactance for different percentages of dynamic loads (90 %, 50%, and 25 %) without the PV plant. As shown, the relay impedance (especially reactance) decreases with decreasing of the dynamic load percentage. For example, at R_F=1.3 Ω, if the dynamic load percentage decreases from 90% to 25%, the relay reactance and resistance decrease from 0.3456Ω and 1.6617Ω to 0.3153Ω and 1.4950Ω, respectively. This can be interpreted as follow: Increasing the dynamic load percentage will increase the fault current I_{23} (Fig. 2b) and consequently increase the voltage at bus 2 (relay location). Consequently, the relay impedance increases. This phenomenon is correct for all values of R_F. When the dynamic load percentage decreases from 90% to 25%, for R_F=0 (solid grounded fault), the relay reactance and resistance decrease from 0.3443Ω and 0.2849Ω to 0.3114Ω and 0.2557 Ω, respectively.

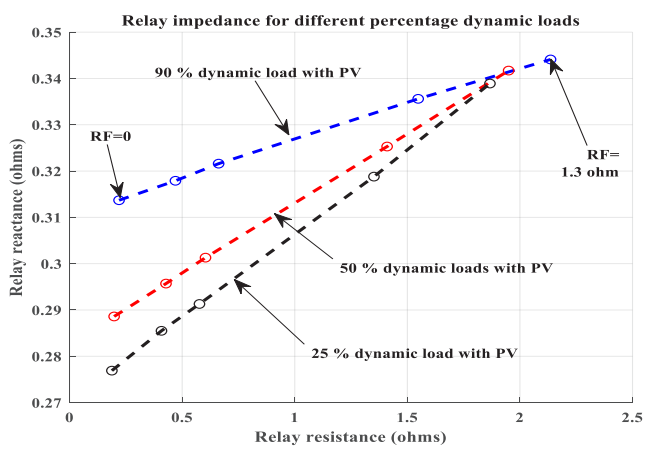

Figure 10. Relay resistance and reactance for different dynamic load percentages with PV.

Fig. 10 shows the relay resistance and reactance for different dynamic load percentages while considering the PV plant fault current. Also, the relay impedance (both resistance and reactance) increases with increasing the

dynamic load percentage in existence of PV plant. For R_F =0 Ω, the impedance relay resistance and reactance increase from 0.1877Ω and 0.2769Ω to 0.219 Ω and 0.3137Ω, respectively. This phenomenon is valid only for small value of the R_F (R_F =0, 0.17, 0.3, and 0.9 Ω) as shown in Fig. 10. As the R_F increases (R_F =1.3 Ω), the dynamic load percentage has a negligible effect on the relay impedance.

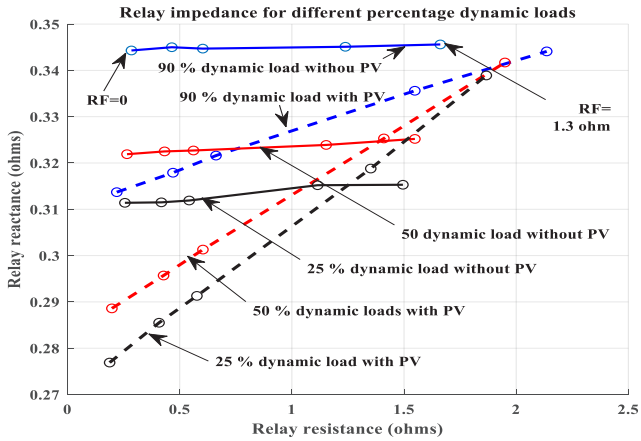

Figure 11. Relay impedance with different dynamic load percentages and different R_F with and without PV for SLG fault at PV bus (bus 3)

Fig. 11 combines the results of both Fig. 9 (without PV) and Fig. 10 (with PV). As shown, the existence of PV reduces the impedance (resistance and reactance) of the relay. The injected fault current by the interfacing inverter of the PV plant increases the total fault current. Consequently, the relay impedance decreases ($Z_{\text{Re}lay} = \frac{V_2}{I_{23}}$). For example, for 90% dynamic loads and R_F =0 Ω, the relay resistance and reactance decrease from 0.2849Ω and 0.3443 Ω (without PV plant) to 0.2195Ω and 0.3137Ω (with PV), as shown in Fig. 11. This phenomenon is valid for small value of R_F . As the R_F increases, the injected fault current by the PV plant has small effect in the relay reading.

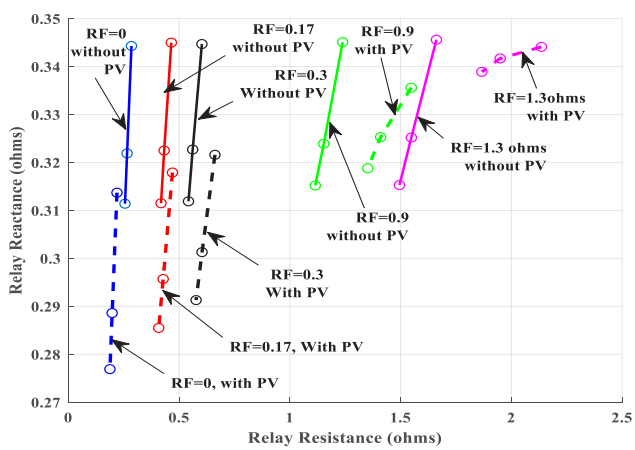

Figure 12. Relay impedance with different dynamic load percentages and different R_F (R_F =0 to R_F =1.3 ohm) with and without PV for SLG fault at PV bus (bus 3).

Fig. 12 displays the effects of dynamic load percentage on the impedance relay resistance and reactance at constant R_F without and with considering the PV plant. As shown, the relay impedance increases with the increase of dynamic load percentages for the same fault resistance with and without considering the PV plant. For high R_F, the existence of the PV plant has a small effect on the relay reading.

5.2 Three Line to Ground Fault at PV Bus for Different Dynamic Loads Percentages with and Without PV (Different Values of R_F)

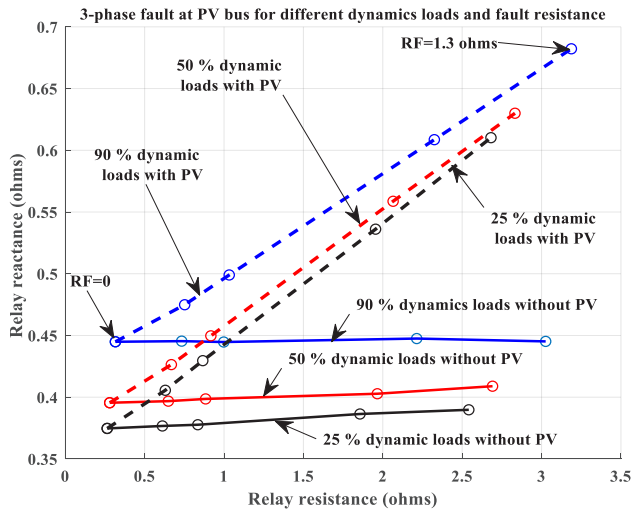

Figure 13. Impedance relay reading for 3-phase fault at PV bus for different percentages of dynamic load and R_F with and without PV.

Fig. 13 shows the relay reading for three line to ground fault at bus 3 with and without PV under different percentage of dynamic load and different values of R_F. As shown, the dynamic load increases the resistance and reactance of the protective impedance relay. The injected fault current by the dynamic load flows through the line from bus 2 to bus 3 and flows through the fault resistance (R_F). This increases the voltage at the relay location (bus 2) and consequently increases the relay impedance as shown in Fig. 13. Without existence of the PV plant, the relay impedance for 90% dynamic load (solid blue line) is larger than its value for 25% dynamic load (solid black line).

With considering the PV plant, the injected fault current by the PV plant flows through the fault resistance and increases the voltage at the relay location (bus 2). The relay impedance increases with the existence of the PV plant. For 90% dynamic load and fault resistance R_F =1.3Ω, the relay resistance and reactance increase from 3.0259 Ω and 0.4452 Ω (without PV) to 3.1877Ω and 0.6822 Ω (with PV), respectively.

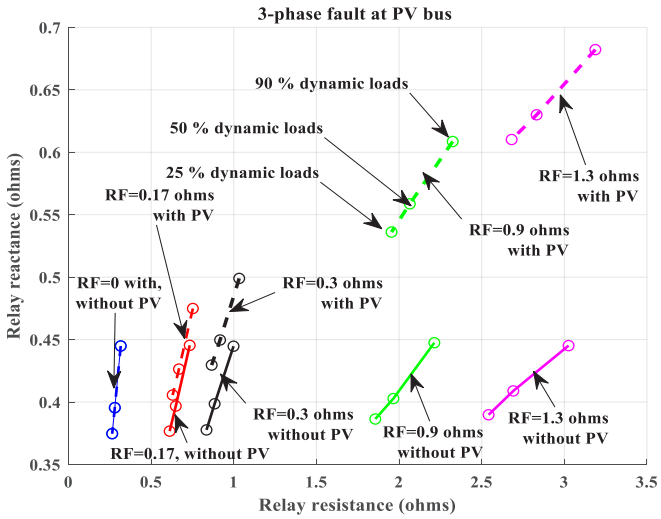

Figjure 14. Relay impedance for 3-line to ground fault at PV bus (bus 3) for constant R_F

Fig. 14 shows the effect of fault resistance on the relay impedance at different dynamic loads with and without the PV plant. As shown, for a high fault resistance (R_F), the PV plant has dominant effect on the protective relay impedance (Fig. 14, violet lines solid and dashed). For small value of R_F, the percentage of both the dynamic load and the PV plant has a negligible effect in the protective relay reading (Blue lines in Fig. 14).

5.3 Single line to ground fault at load bus for different dynamic load percentages with and without PV (different R_F)

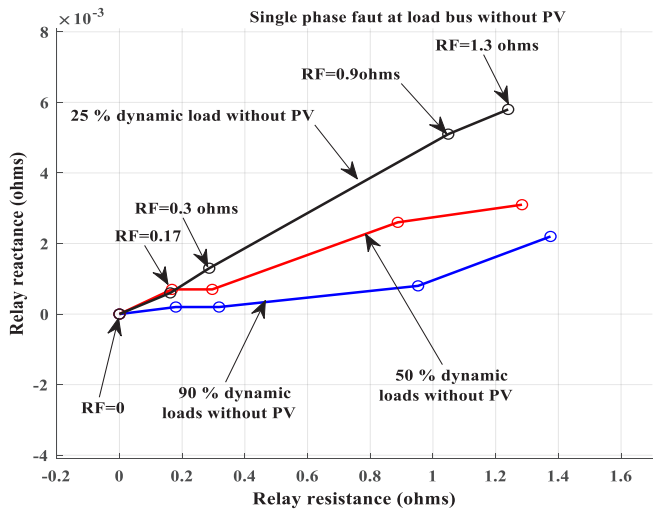

Figure 15. Single line to ground fault at load bus for different dynamic load percentage without PV.

Fig. 15 shows the impedance relay reading during single line to ground fault at load bus (bus 2) without PV and for different dynamic load percentages. As shown, unlike the obtained results for single line to ground fault at PV

bus (Fig. 9), the relay impedance decreases with increasing the dynamic load percentage. When the fault is at load bus (bus 2), the increase in the dynamic load percentage increases the fault current only and does not increase the relay voltage (V_2). Consequently, the relay impedance decreases with the increasingly dynamic load percentage. For example, when the dynamic load percentage increases from 25% to 90%, the resistance and reactance of the relay decreases from 1.0488Ω and 0.0051Ω to 0.9526Ω and 0.0008Ω, respectively. This phenomenon is valid for all values of R_F.

Fig. 16 shows the relay resistance and reactance for single phase to ground fault at load bus, different dynamic loads with considering the PV plant. The increasing in the dynamic load percentage decreases the relay impedance in existence of the PV plant.

Fig. 17 combines both Fig. 15 and Fig. 16 to investigate the effect of the PV plant on the impedance relay reading during single line to ground fault occurrence far from the PV plant bus (load bus). As shown in Fig. 2b, when the fault occurs at the load bus (bus 2), the PV injects fault current (I_{32}). This current flows in the line between PV bus (bus 3) and fault bus (bus 2) cause an improvement to the load bus voltage (V_2), which increases the relay impedance. For example, at 90% dynamic load (blue lines in Fig. 17) and R_F = 1.3 Ω, the relay resistance and reactance increase from 1.375Ω and 0.0022Ω (without PV) to 1.5745Ω and 0.0726Ω (with PV), respectively.

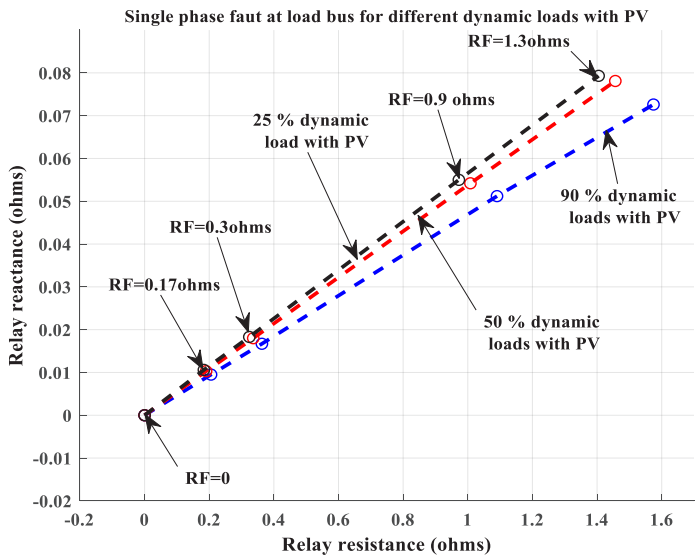

Figure 16. Single line to ground fault at load bus for different dynamic loads with PV.

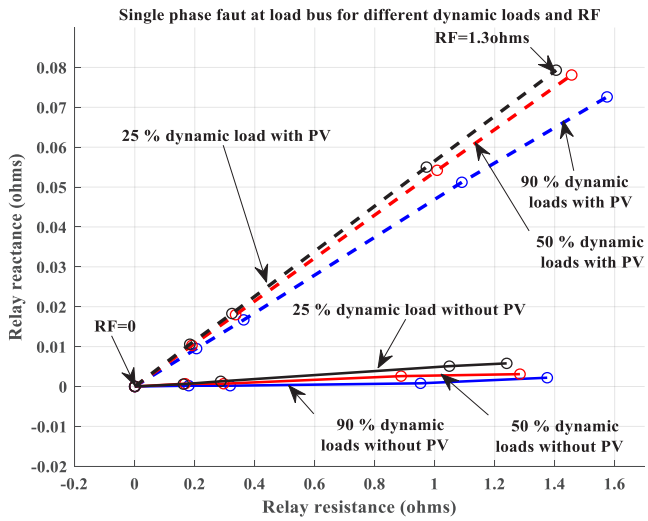

Figure 17. Single line to ground fault at load bus for different percentages of dynamic load and different R_F with and without PV.

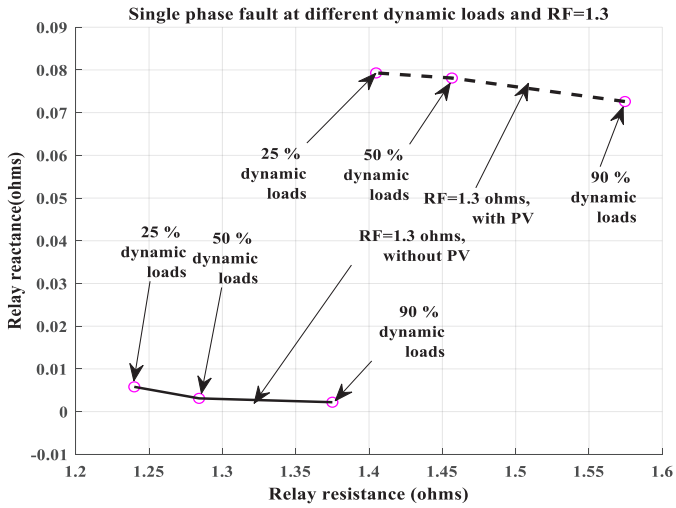

Figure 18. Single line to ground fault at load bus with different percentages of dynamic loads, and constant R_F (R_F=1.3 Ω), with and without PV.

Fig. 18 indicates the effect of both dynamic load percentages and PV plant on the relay reading for constant R_F (R_F=1.3 Ω). The PV plant has a dominant effect on the protective relay reading (both relay resistance and relay reactance) when the fault resistance is held constant. The dynamic load percentage has a considerable effect only on the relay resistance, as well as a negligible effect on the relay reactance.

5.4 Three Lines to Ground Fault at Load Bus With Different Dynamic Load Percentages with and Without PV (different R_F)

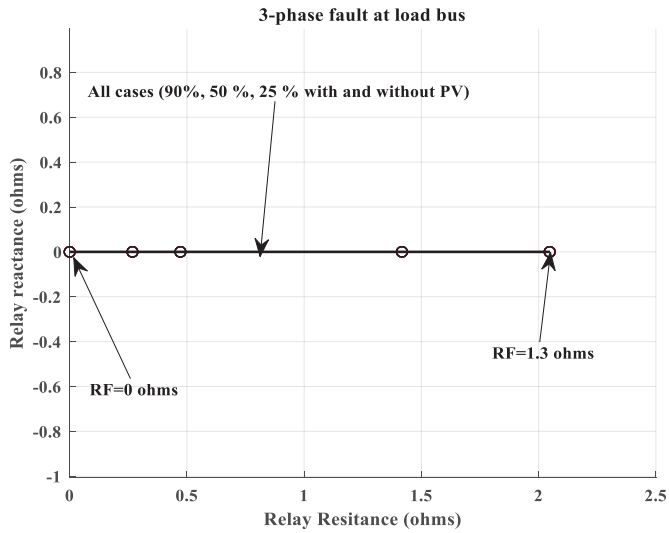

Figure 19. Relay impedance for 3-phase fault at load bus (all cases).

Fig. 19 displays the relay resistance and relay reactance for three line to ground fault at load bus (relay location). As shown, for all cases, the relay reactance equal to zero. The relay has resistance that only depends on the fault resistance (R_F) where $V_2 = I_{SC} R_F$. For three-phase fault at the relay bus, both the dynamic load percentage and the PV plant have no effect on the relay reading. With other words, the relay reading is only dependent on the fault resistance (R_F) for three phase symmetrical fault at its location.

6. CONCLUSION

This paper investigates in detail the effects of both dynamic load percentages and PV plant on the reading and setting of the protective impedance relay. Both balanced (three lines to ground) and unbalanced (single line to ground) faults at different buses (PV bus and load bus) are analyzed. If the fault occurs at the PV system's bus when no PV power is generated (during night), the dynamic load increases the relay impedance, while connecting the PV decreases the relay impedance. The resistance and reactance of the relay increase from 0.3153Ω and 1.4950Ω, to 0.3456Ω and 1.6617Ω, respectively, when the dynamic load increases from 25% to 90% of the total load. The resistance and reactance of the relay decrease from 0.2849Ω and 0.3443Ω (without PV plant), to 0.2195Ω and 0.3137Ω (with PV), respectively. When the dynamic load percentage increases from 25% to 90%, the resistance and reactance of the relay decrease from 1.0488Ω and 0.0051Ω, to 0.9526Ω and 0.0008Ω, respectively. This phenomenon is valid for all expected fault resistances. When considering constant dynamic load percentage and constant fault resistance, the relay resistance and reactance increase from 1.375Ω and 0.0022Ω (without PV) to 1.5745Ω and 0.0726 Ω (with PV), respectively. Based on those results, the impedance relay setting must be adjusted according to the percentage of the dynamic loads, the PV penetration level, and the fault location. The main conclusion of this paper is that both the load type (especially dynamic load) and the PV plant have considerable effects on the protective impedance relay reading and setting. The distribution system planners and operators must consider the PV plant and types of load during designing, setting, and adjusting the protective impedance relays.

REFERENCES

Abdel-Salam, M., Ahmed, A., Ziedan, H., Kamel, R., Sayed, K., Amery, M., Swify, M., 2012. Analysis of protection system for a microgrid supplying irrigation load in Toshka Area, in: IECON 2012 - 38th Annual Conference on IEEE Industrial Electronics Society. pp. 5602–5606. https://doi.org/10.1109/IECON.2012.6389009

Abdullah, H., Kamel, R., El-Sayed, M., 2016. Design and Analysis of 10MWp Grid Connected PV System Installed West Kuwait. 32nd Eur. Photovolt. Sol. Energy Conf. Exhib. 2055–2063. https://doi.org/10.4229/EUPVSEC20162016-5BV.2.68

Anderson, P.M., 1995. Analysis of Faulted Power Systems. Wiley-IEEE Press.

Boutsika, T.N., Papathanassiou, S.A., 2008. Short-circuit calculations in networks with distributed generation. Electr. Power Syst. Res. 78, 1181–1191. https://doi.org/https://doi.org/10.1016/j.epsr.2007.10.003

Bracale, A., Caramia, P., Carpinelli, G., Di Fazio, A.R., 2017. Modeling the three-phase short-circuit contribution of photovoltaic systems in balanced power systems. Int. J. Electr. Power Energy Syst. 93, 204–215. https://doi.org/https://doi.org/10.1016/j.ijepes.2017.05.032

Chen, L.-H., 2017. Overcurrent protection for distribution feeders with renewable generation. Int. J. Electr. Power Energy Syst. 84, 202–213. https://doi.org/https://doi.org/10.1016/j.ijepes.2016.05.003

Concordia, C., Ihara, S., 1982. Load Representation in Power System Stability Studies. IEEE Trans. Power Appar. Syst. PAS-101, 969–977. https://doi.org/10.1109/TPAS.1982.317163

Darwish, A., Abdel-Khalik, A.S., Elserougi, A., Ahmed, S., Massoud, A., 2013. Fault current contribution scenarios for grid-connected voltage source inverter-based distributed generation with an LCL filter. Electr. Power Syst. Res. 104, 93–103. https://doi.org/https://doi.org/10.1016/j.epsr.2013.06.020

Eltawil, M.A., Zhao, Z., 2010. Grid-connected photovoltaic power systems: Technical and potential problems - A review. Renew. Sustain. Energy Rev. 14, 112–129. https://doi.org/https://doi.org/10.1016/j.rser.2009.07.015

Ghorbani, A., Mozafari, B., Ranjbar, A.M., 2012. Digital distance protection of transmission lines in the presence of SSSC. Int. J. Electr. Power Energy Syst. 43, 712–719. https://doi.org/https://doi.org/10.1016/j.ijepes.2012.05.035

Hernández-Callejo, L., Gallardo-Saavedra, S., Alonso-Gómez, V., 2019. A review of photovoltaic systems: Design, operation and maintenance. Sol. Energy 188, 426–440. https://doi.org/https://doi.org/10.1016/j.solener.2019.06.017

Ibrahim, D.K., Abo El Zahab, E.E.D., Mostafa, S.A.E.A., 2017. New coordination approach to minimize the number of re-adjusted relays when adding DGs in interconnected power systems with a minimum value of fault current limiter. Int. J. Electr. Power Energy Syst. 85, 32–41. https://doi.org/https://doi.org/10.1016/j.ijepes.2016.08.003

IEEE Task Force on Load Representation for Dynamic Performance, 1993. Load representation for dynamic performance analysis (of power systems). IEEE Trans. Power Syst. 8, 472–482. https://doi.org/10.1109/59.260837

Iioka, D., Fujii, T., Orihara, D., Tanaka, T., Harimoto, T., Shimada, A., Goto, T., Kubuki, M., 2019. Voltage reduction due to reverse power flow in distribution feeder with photovoltaic system. Int. J. Electr. Power Energy Syst. 113, 411–418. https://doi.org/https://doi.org/10.1016/j.ijepes.2019.05.059

Kamel, R.M., 2014. Effect of wind generation system types on Micro-Grid (MG) fault performance during both standalone and grid connected modes. Energy Convers. Manag. 79, 232–245. https://doi.org/https://doi.org/10.1016/j.enconman.2013.12.009

Kamel, R.M., Nagasaka, K., 2015. Effect of load type on standalone micro grid fault performance. Appl. Energy 160, 532–540. https://doi.org/https://doi.org/10.1016/j.apenergy.2015.09.044

Karimi, M., Mokhlis, H., Naidu, K., Uddin, S., Bakar, A.H.A., 2016. Photovoltaic penetration issues and impacts in distribution network – A review. Renew. Sustain. Energy Rev. 53, 594–605. https://doi.org/https://doi.org/10.1016/j.rser.2015.08.042

Kim, I.-D., Aggarwal, R.K., 2006. A study on the on-line measurement of transmission line impedances for improved relaying protection. Int. J. Electr. Power Energy Syst. 28, 359–366. https://doi.org/https://doi.org/10.1016/j.ijepes.2006.01.002

Kundur, P., 1994. Power System Stability and Control, Electric P. ed. (McGraw-Hill, Inc.), New York.

Kundur, P., Rogers, G.J., Wong, D.Y., Yan, A., 1993. Extended Transient-Midterm Stability Program: Version 3.0. Volume 1, Executive summary: Final report. Palo Alto, CA, USA.

Madeti, S.R., Singh, S.N., 2017a. Monitoring system for photovoltaic plants: A review. Renew. Sustain. Energy Rev. 67, 1180–1207. https://doi.org/https://doi.org/10.1016/j.rser.2016.09.088

Madeti, S.R., Singh, S.N., 2017b. A comprehensive study on different types of faults and detection techniques for solar photovoltaic system. Sol. Energy 158, 161–185. https://doi.org/https://doi.org/10.1016/j.solener.2017.08.069

Masters, C.L., 2002. Voltage rise: the big issue when connecting embedded generation to long 11 kV overhead lines. Power Eng. J. 16, 5-12(7).

Mishra, P., Pradhan, A.K., Bajpai, P., 2021. Adaptive Distance Relaying for Distribution Lines Connecting Inverter-Interfaced Solar PV Plant. IEEE Trans. Ind. Electron. 68, 2300–2309. https://doi.org/10.1109/TIE.2020.2975462

Morren, J., de Haan, S.W.H., 2007. Short-Circuit Current of Wind Turbines With Doubly Fed Induction Generator. IEEE Trans. Energy Convers. 22, 174–180. https://doi.org/10.1109/TEC.2006.889615

Mortazavi, H., Mehrjerdi, H., Saad, M., Lefebvre, S., Asber, D., Lenoir, L., 2015. A Monitoring Technique for Reversed Power Flow Detection With High PV Penetration Level. IEEE Trans. Smart Grid 6, 2221–2232. https://doi.org/10.1109/TSG.2015.2397887

Nikolaidis, V., Tsimtsios, A., Safigianni, A., 2018. Investigating Particularities of Infeed and Fault Resistance Effect on Distance Relays Protecting Radial Distribution Feeders With DG. IEEE Access 6, 11301–11312.

Soheili, A., Sadeh, J., Bakhshi, R., 2018. Modified FFT based high impedance fault detection technique considering distribution non-linear loads: Simulation and experimental data analysis. Int. J. Electr. Power Energy Syst. 94, 124–140. https://doi.org/https://doi.org/10.1016/j.ijepes.2017.06.035

Sorrentino, E., Navas, G., Orea, E., 2018. Effect of an additional large disturbance during power swings on the impedance seen by the out-of-step blocking function. Int. J. Electr. Power Energy Syst. 99, 79–84. https://doi.org/https://doi.org/10.1016/j.ijepes.2017.12.026

Sulawa, T., Zabar, Z., Czarkowski, D., Birenbaum, L., Lee, S., Ten Ami, Y., 2007. Short Circuit Current of Induction Generators, in: 2007 IEEE International Symposium on Circuits and Systems (ISCAS). pp. 2431–2434. https://doi.org/10.1109/ISCAS.2007.378611

Telukunta, V., Pradhan, J., Agrawal, A., Singh, M., Srivani, S.G., 2017. Protection challenges under bulk penetration of renewable energy resources in power systems: A review. CSEE J. Power Energy Syst. 3, 365–379. https://doi.org/10.17775/CSEEJPES.2017.00030

Tleis, N., 2019. Power systems modelling and fault analysis: Theory and practice, Power Systems Modelling and Fault Analysis: Theory and Practice. Elsevier. https://doi.org/10.1016/C2017-0-02262-0

Tseng, K.-H., Kao, W.-S., Lin, J.-R., 2003. Load model effects on distance relay settings. IEEE Trans. Power Deliv. 18, 1140–1146. https://doi.org/10.1109/TPWRD.2003.817507

Xu, Z.Y., Xu, G., Ran, L., Yu, S., Yang, Q.X., 2010. A New Fault-Impedance Algorithm for Distance Relaying on a Transmission Line. IEEE Trans. Power Deliv. 25, 1384–1392. https://doi.org/10.1109/TPWRD.2010.2042082